

Excitation of soft dipole modes in electron scattering

C.A. Bertulani*

Department of Physics, University of Arizona, Tucson, AZ 85721, USA

Abstract

The excitation of soft dipole modes in light nuclei via inelastic electron scattering is investigated. We show that, under the proposed conditions of the forthcoming electron-ion colliders, the scattering cross sections have a direct relation to the scattering by real photons. The response functions for direct breakup are studied with few-body models. The dependence on final state interactions is exploited. A hydrodynamical model for collective pygmy resonances is developed for light, neutron-rich nuclei. A comparison between direct breakup and collective models is performed. The results of this investigation are important for the planned electron-ion colliders at the GSI and RIKEN facilities.

PACS numbers: 25.30.Fj, 25.20.-x, 24.10.Nz

Keywords: Electron scattering, soft dipole modes, unstable nuclear beams.

*Electronic address: bertulani@physics.arizona.edu

I. INTRODUCTION

Reactions with radioactive beams have attracted great experimental and theoretical interest during the last two decades [1]. Progresses of this scientific adventure were reported on measurements of nuclear sizes [2], the use of secondary radioactive beams to obtain information on reactions for astrophysical interest [3, 4], fusion reactions with neutron-rich nuclei [5, 6], tests of fundamental interactions [7], dependence of the equation of state of nuclear matter on the asymmetry energy [8], and many other research directions. Studies of the structure and stability of nuclei with extreme isospin values provide new insights into every aspect of the nuclear many-body problem. In neutron-rich nuclei far from the valley of β -stability, in particular, new shell structures occur as a result of the modification of the effective nuclear potential. Neutron density distributions become very diffuse and the phenomenon of the evolution of the neutron skin and, in some cases, the neutron halo have been observed.

New areas of studies with nuclei far from the stability line will open up with newly proposed experimental facilities. Among these we quote the FAIR facility at the GSI laboratory in Germany. One of the projects for this new facility is the study of electron scattering off unstable nuclei in an electron-ion collider mode [9]. A similar proposal exists for the RIKEN laboratory facility in Japan [10]. By means of elastic electron scattering, these facilities will become the main tool to probe the charge distribution of unstable nuclei [11, 12]. This will complement the studies of matter distribution which have been performed in other radioactive beam facilities using hadronic probes. Inelastic electron scattering will test the nuclear response to electric and magnetic fields. These facilities will become a breakthrough in accurate measurements of these nuclear properties of unstable nuclei. The reason is that electron scattering is a very clean probe. Its electromagnetic interaction with the nucleus is well understood. Inelastic electron scattering can also be very well described in the Born approximation. Higher order processes are only relevant for the distortion of the electron incoming and outgoing waves, affecting mostly the scattering off heavy nuclei.

Up to now, the electromagnetic response of unstable nuclei far from the stability line has been studied hitherto with Coulomb excitation of radioactive beams impinging on a heavy target [4]. This method has been very useful in determining the electromagnetic response in light nuclei [13]. For neutron-rich isotopes [14] the resulting photo-neutron cross sections

are characterized by a pronounced concentration of low-lying $E1$ strength. The onset of low-lying $E1$ strength has been observed not only in exotic nuclei with a large neutron excess, but also in stable nuclei with moderate proton-neutron asymmetry. The problem with such experiments is that the probe is not very clean. It is well known that the nuclear interaction between projectile and target as well as the long range Coulomb distortion of the energy of the fragments interacting with the target (see, e.g. ref. [15]) are problems of a difficult nature. The nuclear response probed with electron does not suffer from these inconveniences.

One of the most interesting aspects of probing the electromagnetic response of exotic nuclei is the concentration of low-lying $E1$ strength. The interpretation of these peaks has engendered a debate: are these “soft dipole modes” just a manifestation of the loosely-bound character of light neutron-rich nuclei, or are they a manifestation of the excitation of a resonance? [16, 17, 18, 19]. As far as we know, there has not been a definite answer to this simple question. This apparently innocuous question has nonetheless become the center of a even more widespread debate. It is believed that the weak binding of outermost neutrons gives rise to a direct break up of the nucleus and a consequent concentration of the electromagnetic response at low energies. The same weak binding can also lead to soft collective modes. In particular, the pygmy dipole resonance (PR), i.e. the resonant oscillation of the weakly-bound neutron mantle against the isospin saturated proton-neutron core. Its structure, however, remains very much under discussion. The electromagnetic response of light nuclei, leading to their dissociation, has a direct connection with the nuclear physics needed in several astrophysical sites [3, 4, 15]. In fact, it has been shown by Goriely [20] that the existence of pygmy resonances have important implications on theoretical predictions of radiative neutron capture rates in the r-process nucleosynthesis, and consequently to the calculated elemental abundance distribution in the universe.

In this work we study the general features of inelastic electron scattering off light nuclei, in particular their response in the continuum. An assessment of the theory of inelastic electron scattering appropriate for the conditions of electron-ion colliders is presented in section 2. Special emphasis is put on the connection of electron scattering and the scattering by real photons, which will be useful to relate electron scattering and Coulomb dissociation measurements. Section 3 deals with the nuclear response within two and three-body models and their dependence of final state interactions. Section 4 discusses the aspects of low energy

collective modes in halo nuclei and their connection with the response obtained with few-body models. The summary and conclusions will be presented in section 5.

II. INELASTIC ELECTRON SCATTERING

In the plane wave Born approximation (PWBA) the cross section for inelastic electron scattering is given by [21, 22]

$$\frac{d\sigma}{d\Omega} = \frac{8\pi e^2}{(\hbar c)^4} \left(\frac{p'}{p} \right) \sum_L \left\{ \frac{EE' + c^2 \mathbf{p} \cdot \mathbf{p}' + m^2 c^4}{q^4} |F_{ij}(q; CL)|^2 + \frac{EE' - c^2 (\mathbf{p} \cdot \mathbf{q})(\mathbf{p}' \cdot \mathbf{q}) - m^2 c^4}{c^2 (q^2 - q_0^2)^2} [|F_{ij}(q; ML)|^2 + |F_{ij}(q; EL)|^2] \right\} \quad (1)$$

where J_i (J_f) is the initial (final) angular momentum of the nucleus, (E, \mathbf{p}) and (E', \mathbf{p}') are the initial and final energy and momentum of the electron, and $(q_0, \mathbf{q}) = ((E - E')/\hbar c, (\mathbf{p} - \mathbf{p}')/\hbar)$ is the energy and momentum transfer in the reaction. $F_{ij}(q; \Pi L)$ are form factors for momentum transfer q and for Coulomb (C), electric (E) and magnetic (M) multipolarities, $\Pi = C, E, M$, respectively.

Here we will only treat electric multipole transitions. Moreover, we will treat low energy excitations such that $E, E' \gg \hbar c q_0$, which is a good approximation for electron energies $E \simeq 500$ MeV and small excitation energies $\Delta E = \hbar c q_0 \simeq 1 - 10$ MeV. These are typical values involved in the dissociation of nuclei far from the stability line.

Using the Siegert's theorem [23, 24], the form factors in eq. 1 are given by

$$F_{ij}(q; EL) \simeq \frac{cq_0}{q} \sqrt{\frac{L+1}{L}} F_{ij}(q; CL) \quad (2)$$

with

$$\begin{aligned} F_{ij}(q; CL) &= 4\pi i^L \frac{\langle J_f \| Y_L(\hat{\mathbf{r}}) \| J_i \rangle}{\sqrt{2J_i + 1}} \int_0^\infty dr r^2 j_L(qr) \delta\rho_{if}^{(EL)}(r) \\ &\simeq \frac{4\pi (iq)^L}{(2L+1)!!} \frac{\langle J_f \| Y_L(\hat{\mathbf{r}}) \| J_i \rangle}{\sqrt{2J_i + 1}} \int_0^\infty dr r^{2+L} \delta\rho_{if}^{(EL)}(r), \end{aligned} \quad (3)$$

where $\delta\rho_{if}^{(EL)}(r)$ is the L -pole radial charge transition density for nuclear excitation from state i to state f . The last identity in eq. 3 is valid in the long-wavelength approximation. Equation 3 also assumes spherical symmetry so that the total transition density can be written as

$$\delta\rho_{if}^{(EL)}(\mathbf{r}) \equiv \langle J_i L J_f | M_i M M_f \rangle \delta\rho_{if}^{(EL)}(r) Y_{LM}(\hat{\mathbf{r}}), \quad (4)$$

where $\langle J_i L J_f | M_i M M_f \rangle$ is a geometrical (Clebsch-Gordan) coefficient. Note that, for electron scattering, the relation between $F_{ij}(q; EL)$ and $F_{ij}(q; CL)$ in eq. 2 is only valid when $qR \ll 1$, implying small scattering angles (or small momentum transfers q). As pointed out by Schiff [25], for larger scattering angles, the Coulomb multipole tends to be considerably larger than the electric multipole.

For very small scattering angles ($\theta \ll 1$) the PWBA cross section, eq. 1, reduces to [21]

$$\frac{d\sigma}{d\Omega} = \frac{4\pi\sigma_M / (Ze)^2}{1 + (2E/M_A c^2) \sin^2(\theta/2)} \sum_L \left[\frac{1}{2} + \left(\frac{2E}{E_\gamma} \right)^2 \frac{L}{L+1} \sin^2\left(\frac{\theta}{2}\right) + \tan^2\left(\frac{\theta}{2}\right) \right] |F_{ij}(q; EL)|^2 \quad (5)$$

where $\sigma_M = (Ze^2/2E)^2 \cos^2(\theta/2) \sin^{-4}(\theta/2)$ is the Mott cross section and the term $1 + (2E/M_A c^2) \sin^2(\theta/2)$ in the denominator was introduced to account for recoil corrections. M_A is the mass of the nucleus and θ is the electron scattering angle.

Now we introduce a reformulation of the above equations which will allow a simpler interpretation of the succeeding results. For $L \geq 1$, we can rewrite eq. 5 as

$$\frac{d\sigma}{d\Omega dE_\gamma} = \sum_L \frac{dN_e^{(EL)}(E, E_\gamma, \theta)}{d\Omega dE_\gamma} \sigma_\gamma^{(EL)}(E_\gamma), \quad (6)$$

where $\sigma_\gamma^{(EL)}(E_\gamma)$, with $E_\gamma = \hbar c q_0$, is the photo-nuclear cross section for the EL -multipolarity, given by [4]

$$\sigma_\gamma^{(EL)}(E_\gamma) = \frac{(2\pi)^3 (L+1)}{L [(2L+1)!!]^2} \left(\frac{E_\gamma}{\hbar c} \right)^{2L-1} \frac{dB(EL)}{dE_\gamma}. \quad (7)$$

In the long-wavelength approximation, the response function, $dB(EL)/dE_\gamma$, in eq. 7 is given by

$$\frac{dB(EL)}{dE_\gamma} = \frac{|\langle J_f \| Y_L(\hat{\mathbf{r}}) \| J_i \rangle|^2}{2J_i + 1} \left[\int_0^\infty dr r^{2+L} \delta\rho_{if}^{(EL)}(r) \right]^2 \rho(E_\gamma), \quad (8)$$

where $\rho(E_\gamma)$ is the density of final states (for nuclear excitations into the continuum) with energy $E_\gamma = E_f - E_i$. The geometric coefficient $\langle J_f \| Y_L(\hat{\mathbf{r}}) \| J_i \rangle$ and the transition density $\delta\rho_{if}^{(EL)}(r)$ will depend on the nuclear model adopted.

Using eqs. 5 and 3 we get (for $L \geq 1$)

$$\begin{aligned} \frac{dN_e^{(EL)}(E, E_\gamma, \theta)}{d\Omega dE_\gamma} &= \frac{4L}{L+1} \frac{\alpha}{E} \left[\frac{2E}{E_\gamma} \sin\left(\frac{\theta}{2}\right) \right]^{2L-1} \\ &\times \frac{\cos^2(\theta/2) \sin^{-3}(\theta/2)}{1 + (2E/M_{Ac}c^2) \sin^2(\theta/2)} \left[\frac{1}{2} + \left(\frac{2E}{E_\gamma}\right)^2 \frac{L}{L+1} \sin^2\left(\frac{\theta}{2}\right) + \tan^2\left(\frac{\theta}{2}\right) \right]. \end{aligned} \quad (9)$$

One can also define a differential cross section integrated over angles so that

$$\frac{d\sigma_e}{dE_\gamma} = \sum_L \frac{dN_e^{(EL)}(E, E_\gamma)}{dE_\gamma} \sigma_\gamma^{(EL)}(E_\gamma), \quad (10)$$

where

$$\frac{dN_e^{(EL)}(E, E_\gamma)}{dE_\gamma} = 2\pi \int_{E_\gamma/E}^{\theta_m} d\theta \sin\theta \frac{dN_e^{(EL)}(E, E_\gamma, \theta)}{d\Omega dE_\gamma}, \quad (11)$$

and θ_m is the maximum electron scattering angle, which depends on the experimental setup. Notice that the lowest limit in the above integral is $\theta_{\min} = E_\gamma/E$, and not zero. This is equivalent to the condition that the minimum momentum transfer in electron scattering is given by $\Delta E/\hbar c$. Eq. 11 is very useful to plan future electron scattering experiments in ion-electron colliders.

Eqs. 6-11 show that under the conditions of the proposed electron-ion colliders, electron scattering will offer the same information as excitations induced by real photons. The reaction dynamics information is contained in the virtual photon spectrum, eqs. 9 and 11, while the nuclear response dynamics information will be contained in eq. 8. The quantities $dN_e^{(EL)}/d\Omega dE_\gamma$ can be interpreted as the number of equivalent (real) photons incident on the nucleus per unit scattering angle Ω and per unit photon energy E_γ . Note that $E0$ (monopole) transitions do not appear in this formalism. As immediately inferred from eq. 8, for $L = 0$ the response function $dB(EL)/dE_\gamma$ vanishes because the volume integral of the transition density also vanishes in the long-wavelength approximation. But for larger scattering angles the Coulomb multipole matrix elements (CL) in eq. 1 are in general larger than the electric (EL) multipoles, and monopole transitions become relevant [25]. The equivalence in eq. 2 will not be valid under these conditions.

In figure 1 we show the virtual photon spectrum for the $E1$, $E2$ and $E3$ multipolarities for electron scattering off arbitrary nuclei at $E_e = 100$ MeV. These spectra have been obtained from eqs. 9 and 11, assuming a maximum scattering angle of 5 degrees. For simplicity,

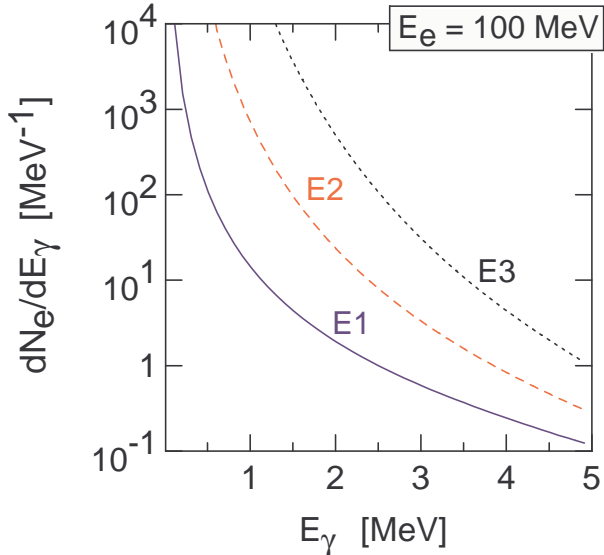


FIG. 1: Virtual photon spectrum for the $E1$, $E2$ and $E3$ multipolarities for electron scattering off arbitrary nuclei at $E_e = 100$ MeV and maximum scattering angle equal to 5 degrees.

the recoil correction has been neglected. An evident feature deduced from this figure is that the spectrum increases rapidly with decreasing energies. Also, at excitation energies of 1 MeV, the spectrum yields the ratios $dN_e^{(E2)}/dN_e^{(E1)} \simeq 500$ and $dN_e^{(E3)}/dN_e^{(E2)} \simeq 100$. However, although $dN_e^{(EL)}/dE_\gamma$ increases with the multipolarity L , the nuclear response decreases rapidly with L , and $E1$ excitations tend to dominate the reaction. For larger electron energies the ratios $N^{(E2)}/N^{(E1)}$ and $N^{(E3)}/N^{(E1)}$ decrease rapidly.

Note that a similar relationship as in eq. 6 also exists for Coulomb excitation [4] in heavy ion scattering. But for Coulomb excitation this factorization is exact for the reason that Coulomb excitation occurs when the nuclei do not overlap. In the electron scattering case, because the electron can also scatter through the nuclear interior, the longitudinal and transverse components of the interaction acquire different weights. To show this we pick up a result first obtained by Bosco and Fubini [26] and later worked out in details by Eisenberg [27] and we relate the results to our present notation.

Let us consider the particle emission from a nucleus following an $E1$ excitation by a real photon. The disintegration cross section for unpolarized photons is given by

$$\frac{d\sigma_\gamma^{E1}}{d\Omega_p} = \frac{1}{4\pi} \left[\sigma_0 + \frac{3}{2} \sigma_1 \sin^2 \vartheta \right], \quad (12)$$

where σ_0 and σ_1 are the part of the photo-dissociation cross section which arises from $M = 0$

and $M = \pm 1$ components of the $\mathcal{M}_{if}(E1M) \sim \langle f | r^L Y_{LM}(\hat{\mathbf{r}}) | i \rangle$ transition matrix elements. In eq. 12, ϑ is the angle of the ejected particle with respect to the direction of the incident photon. The coefficient of the $\sin^2 \vartheta$ term implies that, after an integration over angles of the emitted particle, $\sigma_\gamma^{E1} = \sigma_0 + \sigma_1$. In a disintegration induced by electron scattering, the cross section is also proportional to σ_0 and $\sigma_1 \sin^2 \vartheta$ [27], but the multiplicative factors are not exactly what one would obtain from eqs. 6 and 10.

In our notation one gets

$$\frac{d\sigma_e^{E1}}{dE_\gamma d\Omega_p} = \frac{1}{4\pi} \left[f_0(E, E_\gamma) \sigma_0 + f_1 \sigma_1 + \frac{3}{2} g_1(E, E_\gamma) \sigma_1 \sin^2 \vartheta \right], \quad (13)$$

where

$$f_0(E, E_\gamma) = \frac{1}{\pi E_\gamma} \alpha (\mathcal{L} - 1), \quad f_1 = \frac{9}{4\pi E_\gamma} \alpha, \quad \text{and} \quad g_1(E, E_\gamma) = \frac{1}{\pi E_\gamma} \alpha \left[2\mathcal{L} - \frac{7}{2} \right], \quad (14)$$

and

$$\mathcal{L} = \ln \left(\frac{2E^2}{m_e c^2 E_\gamma} \right). \quad (15)$$

It is obvious that eq. 13 does not factorize as nicely as eq. 10. The argument of the logarithmic function in eq. 15 is large for small excitation energies E_γ (of the order of 1 MeV). Even if we could use $\mathcal{L} \gg 1$ the factor g_1 is about 2 times larger than f_0 .

If we integrate eq. 13 over the angle of the emitted particle, we can recast it to a form similar to eq. 10, i.e.

$$\frac{d\sigma_e^{E1}}{dE_\gamma} = \frac{dN_e^{E10}}{dE_\gamma} \sigma_0 + \frac{dN_e^{E11}}{dE_\gamma} \sigma_1, \quad (16)$$

where

$$\frac{dN_e^{E11}}{dE_\gamma} = \frac{2}{\pi E_\gamma} \alpha \left[\ln \left(\frac{2E^2}{m_e c^2 E_\gamma} \right) - 1 \right] = 2 \frac{dN_e^{E10}}{dE_\gamma}. \quad (17)$$

Neglecting the longitudinal excitations (the term proportional to σ_0), the above equation is in agreement with the results obtained by Bertulani and Baur [4] (their equation 2.6.3a). Following ref. [4] we obtain for the M1 and E2 transitions

$$\frac{dN_e^{M1}}{dE_\gamma} = \frac{dN_e^{E11}}{dE_\gamma} \quad \text{and} \quad \frac{dN_e^{E2}}{dE_\gamma} = \frac{2}{\pi} \alpha \left[\frac{m_e c^2 E_\gamma}{2E^2} + \ln \left(\frac{2E^2}{m_e c^2 E_\gamma} \right) - 1 \right] \simeq \frac{dN_e^{E11}}{dE_\gamma}. \quad (18)$$

In figure 2 we show a comparison between the $E1$ virtual photon spectrum, dN_e/dE_γ , of 1 GeV electrons with the spectrum generated by 1 GeV/nucleon heavy ion projectiles. In the case of Coulomb excitation, the virtual photon spectrum was calculated in ref. [4], eq. 2.5.5a. For simplicity, we use for the strong interaction distance $R = 10$ fm. The spectrum

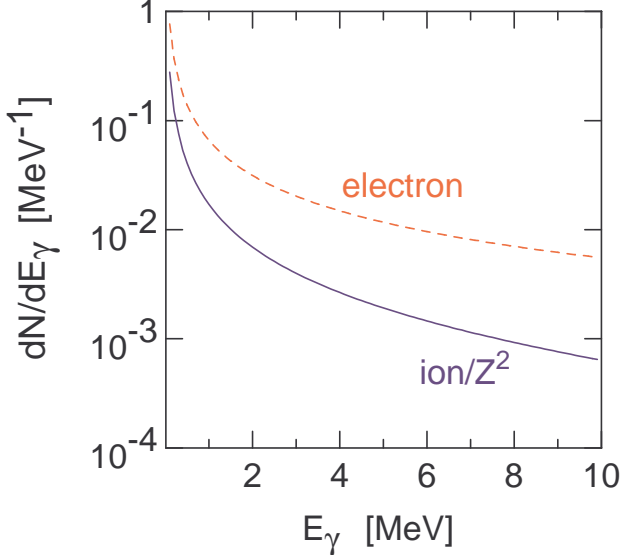


FIG. 2: Comparison between the virtual photon spectrum of 1 GeV electrons (dashed line), and the spectrum generated by a 1 GeV/nucleon heavy ion projectile (solid line) for the $E1$ mutipolarity, as a function of the photon energy. The virtual photon spectrum for the ion has been divided by the square of its charge number.

for the heavy ion case is much larger than that of the electron for large projectile charges. For ^{208}Pb projectiles it can be of the order of 1000 times larger than that of an electron of the same energy. As a natural consequence, reaction rates for Coulomb excitation are larger than for electron excitation. But electrons have the advantage of being a clean electromagnetic probe, while Coulomb excitation at high energies needs a detailed theoretical analysis of the data due to contamination by nuclear excitation. As one observes from figure 2, the virtual spectrum for the electron contains more hard photons, i.e. the spectrum decreases slower with photon energy than the heavy ion photon spectrum. This is because, in both situations, the rate at which the spectrum decreases depends on the ratio of the projectile kinetic energy to its rest mass, E/mc^2 , which is much larger for the electron ($m = m_e$) than for the heavy ion ($m = \text{nuclear mass}$).

III. DISSOCIATION OF WEAKLY-BOUND SYSTEMS

A. One-neutron halo

In this section we will consider the dissociation of a weakly-bound (halo) nucleus from a bound state into a structureless continuum. We will calculate the matrix elements for the response function in eq. 8 in a two-body model. The angular-spin coefficient in eq. 8 which takes into account the coupling between the intrinsic spin, \mathbf{s} , the angular momentum, \mathbf{l} , and the core-spin \mathbf{I} , is given by

$$\frac{|\langle J_f || Y_1 || J_i \rangle|^2}{2J_i + 1} = \frac{3}{4\pi} \hat{l}_i^2 \hat{j}_i^2 \hat{j}_f^2 \hat{l}_f^2 \langle l_i 010 | l_f 0 \rangle^2 \left\{ \begin{array}{ccc} j_i & I & J_i \\ J_f & 1 & j_f \end{array} \right\}^2 \left\{ \begin{array}{ccc} l_i & 1/2 & j_i \\ j_f & 1 & l_f \end{array} \right\}^2, \quad (19)$$

where $\hat{l} = \sqrt{2l+1}$, $\langle \dots \rangle$ is a Clebsch-Gordan coefficient and $\{\dots\}$ are Wigner coefficients.

The single-particle picture has been used previously to study Coulomb excitation of halo nuclei with success [28, 29, 30, 31, 32, 33]. The initial wavefunction can be written as $\Psi_{JM} = r^{-1} u_{ljJ}(r) \mathcal{Y}_{lJM}$, where $R_{ljJ}(r)$ is the radial wavefunction and \mathcal{Y}_{lJM} is a spin-angle function [34]. The radial wavefunction, $u_{ljJ}(r)$, can be obtained by solving of the radial Schrödinger equation for a nuclear potential, $V_{Jlj}^{(N)}(r)$. Some analytical insight maybe obtained by using a simple Yukawa form for an s-wave initial wavefunction, $u_0(r) = A_0 \exp(-\eta r)$, and a p-wave final wavefunction, $u_1(r) = j_1(kr) \cos \delta_1 - n_1(kr) \sin \delta_1$, for the final wavefunction. In these equations η is related to the neutron separation energy $S_n = \hbar^2 \eta^2 / 2\mu$, μ is the reduced mass of the neutron + core system, and $\hbar k = \sqrt{2\mu E_r}$, with E_r being the final energy of the relative motion between the neutron and the core nucleus. A_0 is the normalization constant of the initial wavefunction. The transition density is given by $r^2 \delta \rho_{if}(r) = e_{eff} A_i u_i(r) u_f(r)$, where i and f indices include angular momentum dependence and $e_{eff} = -e Z_c / A$ is the effective charge of a neutron+core nucleus with charge Z_c . The $E1$ transition integral $\mathcal{I}_{l_i l_f} = \int_0^\infty dr r \delta \rho_{if}(r)$ for the wavefunctions described above is

$$\begin{aligned} \mathcal{I}_{s \rightarrow p} &= e_{eff} \frac{2k^2}{(\eta^2 + k^2)^2} \left[\cos \delta_1 + \sin \delta_1 \frac{\eta(\eta^2 + 3k^2)}{2k^3} \right] \\ &\simeq \frac{e_{eff} \hbar^2}{2\mu} \frac{2E_r}{(S_n + E_r)^2} \left[1 + \left(\frac{\mu}{2\hbar^2} \right)^{3/2} \frac{\sqrt{S_n}(S_n + 3E_r)}{-1/a_1 + \mu r_1 E_r / \hbar^2} \right], \end{aligned} \quad (20)$$

where the effective range expansion of the phase shift, $k^{2l+1} \cot \delta \simeq -1/a_l + r_l k^2 / 2$, was used in the second line of the above equation. For $l = 1$, a_1 is the “scattering volume” (units

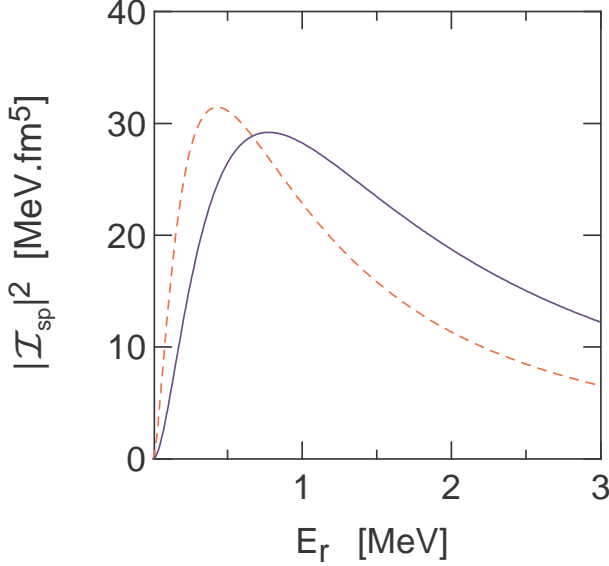


FIG. 3: $|\mathcal{I}_{s \rightarrow p}|^2$ calculated using eq. 20, assuming $e_{eff} = e$, $A = 11$ and $S_n = 0.5$ MeV, as a function of E_r . The solid curve corresponds to $a_1 = -10$ fm $^{-3}$ and $r_1 = 0.5$ fm $^{-1}$ while the dashed curve corresponds to $a_1 = -50$ fm $^{-3}$ and $r_1 = 1$ fm $^{-1}$.

of length 3) and r_1 is the “effective momentum” (units of 1/length). Their interpretation is not as simple as the $l = 0$ effective range parameters. Typical values are, e.g. $a_1 = -13.82$ fm $^{-3}$ and $r_1 = -0.419$ fm $^{-1}$ for n+ 4 He $p_{1/2}$ -wave scattering and $a_1 = -62.95$ fm $^{-3}$ and $r_1 = -0.882$ fm $^{-1}$ for n+ 4 He $p_{3/2}$ -wave scattering [35].

The form of the energy dependence of eq. 20 has some unique features. As shown in previous works [28, 29], the matrix elements for electromagnetic response of weakly-bound nuclei present a small peak at low energies, due to the proximity of the bound state to the continuum. This peak is manifest in the response function of eq. 8:

$$\frac{dB(EL)}{dE} \propto |\mathcal{I}_{s \rightarrow p}|^2 \propto \frac{E_r^{L+1/2}}{(S_n + E_r)^{2L+2}}. \quad (21)$$

It appears centered at the energy [29]

$$E_0^{(EL)} \simeq \frac{2L+1}{L+3/2} S_n \quad (22)$$

for a generic electric response of multipolarity L . For the E1 excitations, the peak occurs at $E_0 \simeq 3S_n/5$.

The second term inside brackets in eq. 20 is a modification due to final state interactions. This modification may become important, as shown in figure 3, where $|\mathcal{I}_{s \rightarrow p}|^2$ calculated with

eq. 20 is plotted as a function of E_r . Here, for simplicity, we have assumed the values $e_{ff} = e$, $A = 11$ and $S_n = 0.5$ MeV. This does not correspond to any known nucleus and it is used to assess the effect of the scattering length and effective range in the transition matrix element. The solid curve corresponds to $a_1 = -10$ fm $^{-3}$ and $r_1 = 0.5$ fm $^{-1}$ while the dashed curve corresponds to $a_1 = -50$ fm $^{-3}$ and $r_1 = 1$ fm $^{-1}$. Although the effective range expansion is only valid for small values of E_r , it is evident from the figure that the matrix element is very sensitive to the effective range expansion parameters.

The strong dependence of the response function on the effective range expansion parameters makes it an ideal tool to study the scattering properties of light nuclei which are of interest for nuclear astrophysics.

B. Two-neutron halo

Many weakly-bound nuclei, like ^6He or ^{11}Li , require a three-body treatment in order to reproduce the electromagnetic response more accurately. In a popular three-body model, the bound-state wavefunction in the CM system is written as an expansion over hyperspherical harmonics (HH), see e.g. [36],

$$\Psi(\mathbf{x}, \mathbf{y}) = \frac{1}{\rho^{5/2}} \sum_{KLSl_xl_y} \Phi_{KLS}^{l_xl_y}(\rho) \left[\mathcal{J}_{KL}^{l_xl_y}(\Omega_5) \otimes \chi_S \right]_{JM}. \quad (23)$$

Here \mathbf{x} and \mathbf{y} are Jacobi vectors where (see figure 4)

$$\mathbf{x} = \frac{1}{\sqrt{2}} (\mathbf{r}_1 - \mathbf{r}_2), \quad \text{and} \quad y = \sqrt{\frac{2(A-2)}{A}} \left(\frac{\mathbf{r}_1 + \mathbf{r}_2}{2} - \mathbf{r}_c \right), \quad (24)$$

where A is the nuclear mass, \mathbf{r}_1 and \mathbf{r}_2 are the position of the nucleons, and \mathbf{r}_c is the position of the core. The hyperradius ρ determines the size of a three-body state: $\rho^2 = x^2 + y^2$. The five angles $\{\Omega_5\}$ include usual angles (θ_x, ϕ_x) , (θ_y, ϕ_y) which parametrize the direction of the unit vectors $\hat{\mathbf{x}}$ and $\hat{\mathbf{y}}$ and the hyperangle θ , related by $x = \rho \sin \theta$ and $y = \rho \cos \theta$, where $0 \leq \theta \leq \pi/2$.

The hyperspherical harmonics have the explicit form

$$\mathcal{J}_{KLM_L}^{l_xl_y}(\Omega_5) = \phi_K^{l_xl_y}(\theta) Y_{LM_L}^{l_xl_y}(\hat{\mathbf{x}}, \hat{\mathbf{y}}), \quad (25)$$

where $K = l_x + l_y + 2\nu$ ($\nu = 0, 1, 2, \dots$), and

$$Y_{LM_L}^{l_xl_y}(\hat{\mathbf{x}}, \hat{\mathbf{y}}) = [Y_{l_x}(\hat{\mathbf{x}}) \otimes Y_{l_y}(\hat{\mathbf{y}})]_{LM_L}. \quad (26)$$

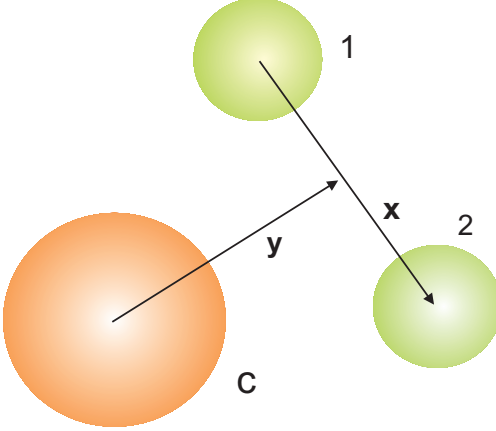


FIG. 4: Jacobian coordinates (\mathbf{x} and \mathbf{y}) for a three-body system consisting of a core (c) and two nucleons (1 and 2).

$Y_{lm}(\hat{\mathbf{x}})$ are the usual spherical harmonics. In eq. 25 the hyperangular functions are given by

$$\phi_K^{l_x l_y}(\theta) = N_K^{l_x l_y} \sin^{l_x} \theta \cos^{l_y} \theta P_n^{l_x + 1/2, l_y + 1/2}(\cos 2\theta) \quad (27)$$

where $P_n^{\alpha, \beta}$ are the Jacobi polynomials, $n = (K - l_x - l_y)/2$ and $N_K^{l_x l_y}$ are normalization constants. The hyperspherical harmonics in eq. 25 are orthonormalized using the volume element $d\Omega_5 = \sin^2 \theta \cos^2 \theta d\hat{\mathbf{x}} d\hat{\mathbf{y}}$. The insertion of the three-body wavefunction, eq. 23, into the Schrodinger equation yields a set of coupled differential equations for the hyperradial wavefunction $\Phi_{KLS}^{l_x l_y}(\rho)$. Assuming that the nuclear potentials between the three particles are known, this procedure yields the bound-state wavefunction for a three-body system with angular momentum J .

In order to calculate the electric response we need the scattering wavefunctions in the three-body model to calculate the integrals in eq. 8. One would have to use final wavefunctions with given momenta, including their angular information. When the final state interaction is disregarded these wavefunctions are three-body plane waves [38, 39]. To carry out the calculations, the plane waves can be expanded in products of hyperspherical harmonics in coordinate and momentum spaces. However, since we are only interested in the energy dependence of the response function, we do not need directions of the momenta. Thus, instead of using plane waves, we will use a set of final states which just include the coordinate space and energy dependence.

We will also adopt an approach closely related to the work of Pushkin et al. [38] (see also

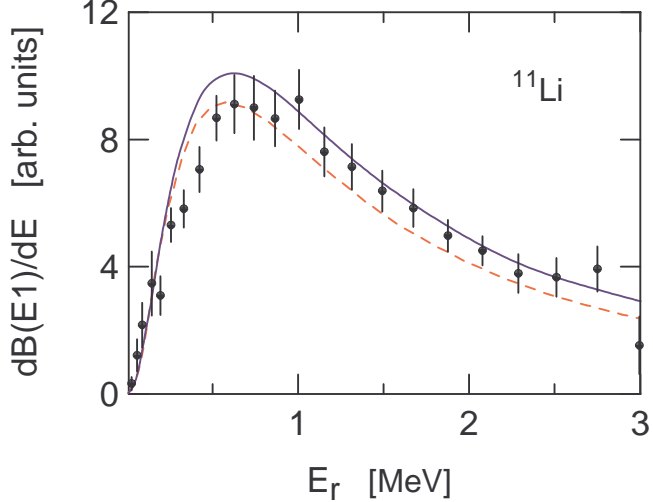


FIG. 5: Comparison between the calculation of the response function (in arbitrary units) with eqs. 29 and 31, using $\delta_{nn} = 0$ and $\delta_{nc} = 0$, (dashed line), or including the effects of final state interactions (continuous line). The experimental data are from ref. [44].

[40, 41]). For weakly-bound systems having no bound subsystems the hyperradial functions entering the expansion 23 behave asymptotically as [37]

$$\Phi_a(\rho) \longrightarrow \text{constant} \times \exp(-\eta\rho), \quad \text{as} \quad \rho \longrightarrow \infty, \quad (28)$$

where the two-nucleon separation energy is related to η by $S_{2n} = \hbar^2\eta^2 / (2m_N)$. This wavefunction has similarities with the two-body case, when ρ is interpreted as the distance r between the core and the two nucleons, treated as one single particle. But notice that the mass m_N would have to be replaced by $2m_N$ if a simple two-body (the dineutron-model [4, 42]) were used for ^{11}Li or ^6He .

Since only the core carries charge, in a three-body model the $E1$ transition operator is given by $M \sim yY_{1M}(\hat{\mathbf{y}})$ for the final state (see also [39]). The $E1$ transition matrix element is obtained by a sandwich of this operator between $\Phi_a(\rho) / \rho^{5/2}$ and scattering wavefunctions. In ref. [38] the scattering states were taken as plane waves. We will use distorted scattering states, leading to the expression

$$\mathcal{I}(E1) = \int dx dy \frac{\Phi_a(\rho)}{\rho^{5/2}} y^2 x u_p(y) u_q(x), \quad (29)$$

where $u_p(y) = j_1(py) \cos \delta_{nc} - n_1(py) \cos \delta_{nc}$ is the core-neutron asymptotic continuum wavefunction, assumed to be a p -wave, and $u_q(x) = j_0(qx) \cos \delta_{nn} - n_0(qx) \cos \delta_{nn}$ is the

neutron-neutron asymptotic continuum wavefunction, assumed to be an s -wave. The relative momenta are given by

$$\mathbf{q} = \frac{1}{\sqrt{2}} (\mathbf{q}_1 - \mathbf{q}_2), \quad \text{and} \quad \mathbf{p} = \sqrt{\frac{2(A-2)}{A}} \left(\frac{\mathbf{k}_1 + \mathbf{k}_2}{2} - \mathbf{k}_c \right). \quad (30)$$

The $E1$ strength function is proportional to the square of the matrix element in eq. 29 integrated over all momentum variables, except for the total continuum energy $E_r = \hbar^2 (q^2 + p^2) / 2m_N$. This procedure gives

$$\frac{dB(E1)}{dE_r} = \text{constant} \times \int |\mathcal{I}(E1)|^2 E_r^2 \cos^2 \Theta \sin^2 \Theta d\Theta d\Omega_q d\Omega_p, \quad (31)$$

where $\Theta = \tan^{-1}(q/p)$.

The 1S_0 phase shift in nucleon-nucleon scattering is remarkably well reproduced up to center of mass energy of order of 5 MeV by the first two terms in the effective-range expansion $k \cot \delta_{nn} \simeq -1/a_{nn} + r_{nn}k^2/2$. Experimentally these parameters are determined to be $a_{nn} = -23.7$ fm and $r_{nn} = 2.7$ fm. The extremely large (negative) value of the scattering length implies that there is a virtual bound state in this channel very near zero energy. The p-wave scattering in the n- ${}^9\text{Li}$ (${}^{10}\text{Li}$) system appears to have resonances at low energies [43]. We will assume that this phase-shift can be described by the resonance relation

$$\sin \delta_{nc} = \frac{\Gamma/2}{\sqrt{(E_r - E_R)^2 + \Gamma^2/4}}, \quad (32)$$

with $E_R = 0.53$ MeV and $\Gamma = 0.5$ MeV [43].

Most integrals in eqs. 29 and 31 can be done analytically, leaving two remaining integrals which can only be performed numerically. The result of the calculation is shown in figure 5. The dashed line was obtained using $\delta_{nn} = 0$ and $\delta_{nc} = 0$, that is, by neglecting final state interactions. The continuous curve includes the effects of final state interactions, with δ_{nn} and δ_{nc} parametrized as described above. The experimental data are from ref. [44]. The data and theoretical curves are given in arbitrary units. Although the experimental data is not perfectly described by either one of the results, it is clear that final state interactions are of extreme relevance.

As pointed out in ref. [38], the $E1$ three-body response function of ${}^{11}\text{Li}$ can still be described by a form similar to eq. 21, but with different powers. Explicitly,

$$\frac{dB(E1)}{dE_r} \propto \frac{E_r^3}{(S_{2n}^{eff} + E_r)^{11/2}}. \quad (33)$$

But instead of S_{2n} , one has to use an effective $S_{2n}^{eff} = aS_{2n}$, with $a \simeq 1.5$. With this approximation, the peak of the strength function in the three-body case obtained from eq. 33 is situated at about three times higher energy than for the two-body case, eq. 21. In the three-body model, the maximum is thus predicted at $E_0^{(E1)} \simeq 1.8S_{2n}$, which fits the experimentally determined peak position for the ^{11}Li $E1$ strength function very well [38]. It is thus apparent that the effect of three-body configurations is to widen and to shift the strength function $dB(E1)/dE$ to higher energies.

IV. COLLECTIVE EXCITATIONS: THE PIGMY RESONANCE

A. The hydrodynamical model

Hitherto we have discussed the direct dissociation of loosely-bound nuclei. We have seen that the energy position where the soft dipole response peaks depends on the few body model adopted. Except for a two-body resonance in ^{10}Li , there was no reference to a resonance in the continuum in the previous sections. The peak in the response function can be simply explained by the fact that it has to grow from zero at low energies and return to zero at large energies. In few-body, or cluster, models, the form of the bound-state wavefunctions and the phase space in the continuum determine the position of the peak in the response function. Few-body resonances will add extra peaks to it.

Now we will consider the case in which a collective resonance is present. As in the case of giant dipole resonances (GDR) in stable nuclei, one believes that pygmy resonances at energies close to the threshold are present in halo, or neutron-rich, nuclei. This was proposed by Suzuki et al. [45] using the hydrodynamical model for collective vibrations. The possibility to explain the soft dipole modes (figure 5) in terms of a direct breakup, has made it very difficult to clearly identify the signature of pygmy resonances in light exotic nuclei. We shall consider next how the response function behaves when calculated in the hydrodynamical model.

The hydrodynamical model, first suggested by Goldhaber and Teller [46] and by Steinwedel and Jensen [47] needs adjustments to explain collective response in light, neutron-rich, nuclei. Because clusterization in light nuclei exists, not all neutrons and protons can be treated equally. The necessary modifications are straight-forward and discussed next,

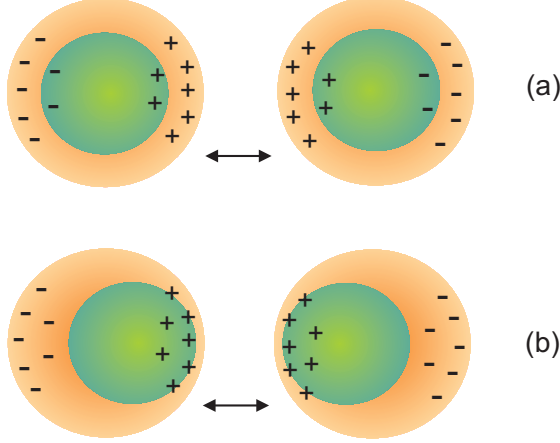


FIG. 6: Hydrodynamical model for collective nuclear vibrations in a halo nucleus. The (a) Steinwedel-Jensen (SJ) mode and the (b) Goldhaber-Teller (GT) mode are shown separately.

starting with the case of large stable nuclei. To our knowledge, the radial dependence of the transition densities in the hydrodynamical model for light, neutron-rich, nuclei has not been discussed in the literature. We will use the method of Myers et al. [48], who considered the collective vibrations in nuclei as an admixture of Goldhaber-Teller and Steinwedel-Jensen modes. For light nuclei they found that the Goldhaber-Teller mode dominates. But in order to reproduce the correct position of the GDR along the periodic table both modes have to be included.

When a collective vibration of protons against neutrons is present in a nucleus with charge (neutron) number Z (N), in a given position \mathbf{r} inside the nucleus, the velocity of the neutron fluid, \mathbf{v}_n , and of the proton fluid, \mathbf{v}_p , are given in the hydrodynamical model by

$$\mathbf{v}_p = \frac{N}{A}\mathbf{v} = \frac{N}{A}(\mathbf{v}_1 + \mathbf{v}_2), \quad \text{and} \quad \mathbf{v}_n = -\frac{Z}{A}\mathbf{v} = -\frac{Z}{A}(\mathbf{v}_1 + \mathbf{v}_2), \quad (34)$$

where the factors N/A and $(-Z/A)$ are used to account for the motion of the center-of-mass of the combined fluids, which is not of interest.

The velocity \mathbf{v}_1 , of the Goldhaber-Teller fluid is, in Cartesian coordinates, given by

$$\mathbf{v}_1 = \dot{\alpha}_1 R (\cos \theta \hat{\mathbf{e}}_r - \sin \theta \hat{\mathbf{e}}_\theta) \quad (35)$$

where θ is the polar angle with respect to the symmetry axis, R is the mean nuclear radius of the nucleus, α_1 represents the percent displacement of the center of mass of the neutron and proton fluids in the Goldhaber-Teller (GT) mode, and $\hat{\mathbf{e}}_r$ and $\hat{\mathbf{e}}_\theta$ are the unit vectors along

the r and θ directions. The neutron and proton fluids are displaced with respect to each other by $d_1 = \alpha_1 R$ and each of the fluids are displaced from the origin (center of mass of the system) by $d_p = Nd_1/A$ and $d_n = -Zd_1R/A$. This leaves the center of mass fixed. The dipole moment is given by $D_1 = e \sum_p (\mathbf{r}_p - \mathbf{R})$, where \mathbf{r}_p and \mathbf{R} are the vector positions of a proton and of the center of mass of the nucleus (A, Z). One gets $D_1 = Zed_p = \alpha_1 NZeR/A$. The GT model assumes that the restoring force is due to the increase of the nuclear surface which leads to an extra energy proportional to $A^{2/3}$. In this model, the inertia is proportional to A and the excitation energy is consequently given by $E_x \propto \sqrt{A^{2/3}/A} = A^{-1/6}$.

For a light, weakly-bound nucleus, it is more appropriate to assume that the neutrons inside the core (A_c, Z_c) vibrate in phase with the protons. The neutrons and protons in the core are tightly bound. An overall displacement among them requires energies of the order of 10-20 MeV, well above that of the soft dipole modes. Calling the excess nucleons by $(A_e, Z_e) = (A - A_c, Z - Z_c)$, the dipole moment becomes

$$\begin{aligned} \mathbf{D}_1 &= eZ_c(\mathbf{R}_c - \mathbf{R}) + eZ_e(\mathbf{R}_e - \mathbf{R}) = e\mathbf{d}_1 \frac{[Z_c(A - A_c) - A_c(Z - Z_c)]}{A} \\ &= Z_{eff}^{(1)} e\mathbf{d}_1, \end{aligned} \quad (36)$$

where \mathbf{d}_1 is a vector connecting the center of mass of the two fluids (core and excess neutrons). As before, we can use $d_1 = \alpha_1 R$. We see that the dipole moment is now smaller than before because the effective charge changes from NZ/A in the case of the GDR to $Z_{eff}^{(1)} = (Z_c A_e - A_c Z_e)/A$. This effective charge is zero if $(A_c, Z_c) = (A, Z)$ and no pigmy resonance is possible in this model, only the regular GDRs.

Figure 6 shows a schematic representation of the hydrodynamical model for collective nuclear vibrations in a halo nucleus, as considered here. Part (a) of the figure shows the Steinwedel-Jensen (SJ) mode in which the total matter density of both the core and the halo nucleons do not change locally. Only the local ratio of the neutrons and protons changes. Part (b) of the figure shows a particular case of the Goldhaber-Teller (GT) mode, in which the core as a whole moves with respect to the halo nucleons.

For spherically symmetric densities, the transition density in the GT mode can be calculated from $\delta\rho_p = \rho_p(|\mathbf{r} - \mathbf{d}_p|) - \rho(\mathbf{r})$. Using $d_1 \ll R$, it is straight-forward to show that the charge transition density is

$$\delta\rho_p^{(1)}(\mathbf{r}) = Z_{eff}^{(1)} \alpha_1 R \cos\theta \frac{d\rho_0}{dr} \equiv \delta\rho_p(r) Y_{10}(\hat{\mathbf{r}}), \quad (37)$$

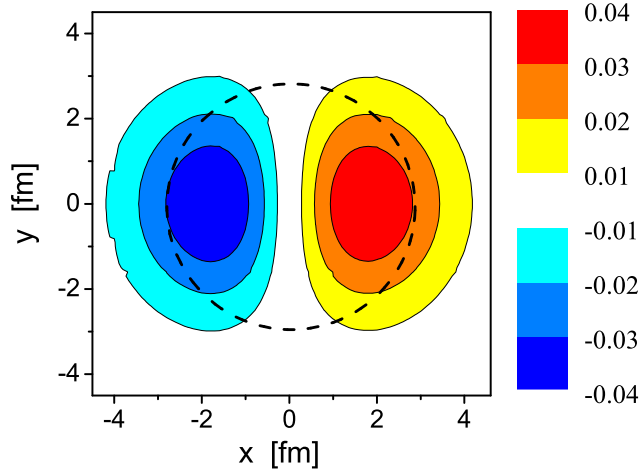


FIG. 7: Contour plot of the nuclear transition density in the hydrodynamical model consisting of a mixture of GT and SJ vibrations. The darker areas represent the larger values of the transition density in a nucleus which has an average radius represented by the dashed circle. The legend on the right displays the values of the transition density within each contour limit.

where ρ_0 is the ground-state density of the nucleus normalized to unity, $\int d^3r \rho_0 = 1$, and

$$\delta\rho_p^{(1)}(r) = \sqrt{\frac{4\pi}{3}} Z_{eff} \alpha_1 R \frac{d\rho_0}{dr}. \quad (38)$$

In the Steinwedel-Jensen (SJ) mode, the velocity \mathbf{v}_2 at a distance r from the center-of-mass of the fluid is given, in polar coordinates, by

$$\mathbf{v}_2 = \dot{\alpha}_2 \frac{K}{k} \left[j'_1(kr) \cos \theta \hat{\mathbf{e}}_r - \frac{1}{kr} j_1(kr) \sin \theta \hat{\mathbf{e}}_\theta \right] \quad (39)$$

where $j(kr)$ is the spherical Bessel function of first order, α_2 the percent displacement of the center of mass of the neutron and proton fluids in the Steinwedel-Jensen mode and

$$kR = a = 2.081, \quad \text{and} \quad K = \frac{2a}{j_0(a)} = 9.93. \quad (40)$$

The relations in eq. 40 are obtained by the condition that the radial velocity of the SJ fluid vanishes at the nuclear surface.

In the SJ mode the local variation of the density of protons is found to be

$$\delta\rho_p^{(2)}(\mathbf{r}) = Z_{eff}^{(2)} \alpha_2 K j_1(kr) \rho_0(r) \cos \theta \equiv \delta\rho_p(r) Y_{10}(\hat{\mathbf{r}}), \quad (41)$$

where

$$\delta\rho_p^{(2)}(r) = \sqrt{\frac{4\pi}{3}}Z_{eff}^{(2)}\alpha_2Kj_1(kr)\rho_0(r). \quad (42)$$

If the proton and neutron content of the core does not change [45], the effective charge number in the SJ mode is given by $Z_{eff}^{(2)} = Z^2(N - N_c)/A(Z + N_c)$.

The transition density at a point \mathbf{r} from the center-of-mass of the nucleus is a combination of the SJ and GT distributions and is given approximately by

$$\begin{aligned} \delta\rho_p(\mathbf{r}) &= \delta\rho_p^{(1)}(\mathbf{r}) + \delta\rho_p^{(2)}\mathbf{r} \\ &= R\cos\theta\left[Z_{eff}^{(1)}\alpha_1\frac{d\rho_0(r)}{dr} + Z_{eff}^{(2)}\alpha_2\frac{K}{R}j_1(kr)\rho_0(r)\right], \\ &= \delta\rho_p(r)Y_{10}(\hat{\mathbf{r}}), \end{aligned} \quad (43)$$

where

$$\delta\rho_p(r) = \sqrt{\frac{4\pi}{3}}R\left\{Z_{eff}^{(1)}\alpha_1\frac{d}{dr} + Z_{eff}^{(2)}\alpha_2\frac{K}{R}j_1(kr)\right\}\rho_0(r). \quad (44)$$

Changes can be done to these expressions to account for the different radii of the proton and neutron densities.

In figure 7 we show the contour plot of the nuclear transition density in the hydrodynamical model, eq. 43 consisting of a mixture of GT and SJ vibrations. The darker areas represent the larger values of the transition density in a nucleus which has an average radius represented by the dashed circle. In this particular case, we used the HF density [12, 49] for ^{11}Li , and used a radius $R = 3.1$ fm. The parameters α_1 and α_2 were chosen so that $Z_{eff}^{(1)}\alpha_1 = Z_{eff}^{(2)}\alpha_2$, i.e. a symmetric mixture of the SJ and GT modes. The unit for $\delta\rho_p(r)$ shown in the figure is arbitrary.

In figure 8 we show the transition densities for the ^{11}Li for three different assumptions of the SJ+GT admixtures, according to our formula, eq. 44. The dashed curve is for a GT oscillation mode, with the core vibrating against the halo neutrons, with effective charge number $Z_{eff}^{(1)} = 6/11$, radius $R = 3.1$ fm, and $\alpha_1 = 1$. The dotted curve is for an SJ oscillation mode, with effective charge number $Z_{eff}^{(2)} = 2/11$, and $\alpha_2 = 1$. The solid curve is the sum of the previous two. Notice that the transition densities are peaked at the surface, but at a radius smaller than the adopted ‘rms’ radius $R = 3.1$ fm. Had we used a homogeneous distribution of charge and nucleon matter, with a sharp-cutoff radius R , then $\delta\rho_p^{(1)}(\mathbf{r}) \propto \delta(r - R)$, and $\delta\rho_p^{(2)}(\mathbf{r}) \propto j_1(kr)\Theta(r - R)$, where $\delta(r - R)$ is the delta-function

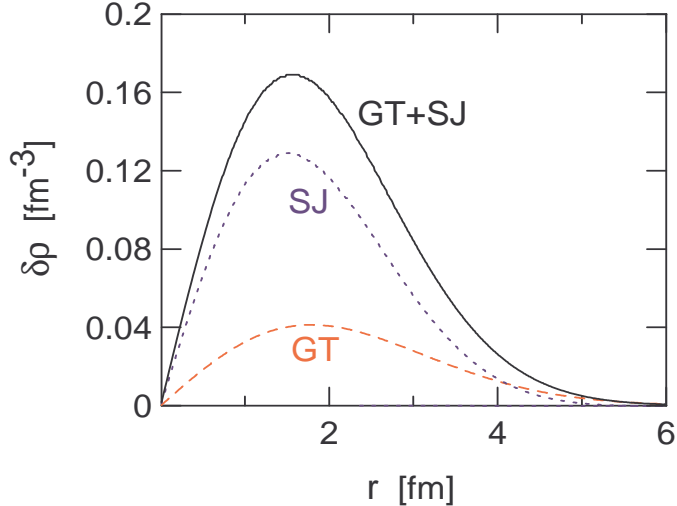


FIG. 8: Hydrodynamical transition densities for ^{11}Li for three different assumptions for the SJ+GT admixtures, according to eq. 44. The dashed curve is for a GT oscillation mode, with the core vibrating against the halo neutrons, with effective charge number $Z_{eff}^{(1)} = 6/11$, radius $R = 3.1$ fm, and $\alpha_1 = 1$. The dotted curve is for an SJ oscillation mode, with effective charge number $Z_{eff}^{(2)} = 2/11$, and $\alpha_2 = 1$. The solid curve is the sum of the two.

and $\Theta(r - R)$ the step function. The transition density for the later case (SJ mode) still has spatial variations due to the presence of the spherical Bessel function $j_1(kr)$.

The hydrodynamical model can be further explored to obtain the energy and excitation strength of the collective excitations, as was done by Myers et al. [48] for the giant dipole resonances and by Suzuki et al. [45] for the pygmy resonances in neutron-rich nuclei. This can be done by finding the eigenvalues of the Hamiltonian

$$\mathcal{H} = \frac{1}{2}\dot{\alpha}\mathcal{T}\dot{\alpha} + \frac{1}{2}\alpha\mathcal{V}\alpha + \dot{\alpha}\mathcal{F}\dot{\alpha}, \quad (45)$$

where $\alpha = (\alpha_1, \alpha_2)$ is now a vector containing the GT and SJ contributions to the collective motion. T and V are the kinetic and potential energies 2×2 matrices [48].

The first term in eq. 45 can be calculated from the velocity fields of eqs. 35 and 39 as follows:

$$T = \frac{1}{2}m_N^* \int [\rho_p (\mathbf{v}_{1p} + \mathbf{v}_{2p})^2 + \rho_n (\mathbf{v}_{1n} + \mathbf{v}_{2n})^2] d^3r, \quad (46)$$

where the effective nucleon mass m_N^* accounts for the meson exchange effects.

The second term of eq. 45 can be related to the stiffness parameters of the liquid-drop

model adjusted to a best fit to the nuclear masses. The stiffness of the system is due to the change in symmetry energy of the system as it goes out of the equilibrium position:

$$V = -\kappa \int \frac{(\rho_p - \rho_n)^2}{\rho_p + \rho_n} d^3r, \quad (47)$$

where κ can be estimated from the semi-empirical mass formula ($\kappa \simeq 30 - 40$ MeV). The last term in equation 45 is the Rayleigh dissipation term, which can be related to the Fermi velocity of the nucleons [48]. By diagonalizing the first two parts of the Hamiltonian in eq. 45 one obtains the eigenstate energies of the GT+SJ collective mode, and the relative values of α_1 and α_2 . The last term of eq. 45 yields the width of the eigenstate.

As shown by Myers et al. [48], the liquid drop model predicts an equal admixture of SJ+GT oscillation modes for large nuclei. The contribution of the SJ oscillation mode decreases with decreasing mass number, i.e. $\alpha \rightarrow (\alpha_1, 0)$ as $A \rightarrow 0$. This is even more probable in the case of halo nuclei, where a special type of GT mode (the oscillations of the core against the halo nucleons) is likely to be dominant. For this special collective motion an approach different than those used in refs. [48] and [45] has to be considered. For simplicity, we shall here follow the original arguments by Goldhaber and Teller [46].

It is easy to make changes in the original Goldhaber and Teller [46] formula for the energy of the collective vibrations. One has to account for the effective mass of our modified GT model. The resonance energy formula derived by Goldhaber and Teller [46] becomes

$$E_{PR} = \left(\frac{3\varphi\hbar^2}{2aRm_N A_r} \right)^{1/2}, \quad (48)$$

where $A_r = A_c(A - A_c)/A$ and a is the length within which the interaction between a neutron and a nucleus changes from a zero-value outside the nucleus to a high value inside, i.e. a is the size of the nuclear surface. φ is the energy needed to extract one neutron from the proton environment. Goldhaber and Teller [46] argued that in a heavy stable nucleus φ is not the binding energy of the nucleus, but the part of the potential energy due to the neutron proton interaction. It is proportional to the asymmetry energy. In the case of weakly-bound nuclei this picture changes and it is more reasonable to associate φ to the separation energy of the valence neutrons, S . We will use $\varphi = \beta S$, with a parameter β which is expected to be of order of one. Since for halo nuclei the product aR is proportional to S^{-1} , we obtain the proportionality $E_{PR} \propto S$. Due to the simplicity of the model, the proportionality factor cannot be trusted. Using eq. 48 for ^{11}Li , with $a = 1$ fm, $R = 3$ fm

and $\varphi = S_{2n} = 0.3$ MeV, we get $E_{PR} = 1.3$ MeV. Considering that the pygmy resonance will most probably decay by particle emission, one gets $E_r \simeq 1$ MeV for the kinetic energy of the fragments. This is about a factor 2 larger than what is observed as the position of the peak in figure 5. But it is within the right ballpark.

It is possible that the formula 48 for the energy of the pigmy collective vibrations can be improved by the calculation of eqs. 46 and 47, using proton and neutron density profiles obtained from microscopic calculations. It must be remembered, however, that the hydrodynamical model is very unlikely to be an accurate model for light, loosely-bound, nuclei and is significant only in that the correct order of magnitude of the resonance energy is found.

The main decay channel of the pigmy resonance is the breakup of the nucleus. As shown above, both the direct dissociation model and the hydrodynamical model yield a bump in the response function proportional to S , the valence nucleon(s) separation energy. What about the width of the response function, as observed in figure 5? In the direct dissociation model the width of the response function obviously depends on the separation energy. But it also depends on the nature of the model, i.e. if it is a two-body model, like the model often adopted for ^{11}Be or ^8B , or a three-body model, appropriate for ^{11}Li and ^6He . In the two-body model the phase-space depends on energy as $\rho(E) \propto d^3p/dE \propto \sqrt{E}$, while for in the three-body model $\rho(E) \sim E^2$. This explains why the peak of figure 5 is pushed toward higher energy values, as compared to the prediction of eq. 21. It also explains the larger width of dB/dE obtained in three-body models. In the case of the pigmy resonance, this question is completely open.

The hydrodynamical model predicts [48] for the width of the collective mode $\Gamma = \hbar \bar{v}/R$, where \bar{v} is the average velocity of the nucleons inside the nucleus. This relation can be derived by assuming that the collective vibration is damped by the incoherent collisions of the nucleons with the walls of the nuclear potential well during the vibration cycles. This approach mimics that used in the kinetic theory of gases for calculating the energy transfer of a moving piston to gas molecules in a container. Using $\bar{v} = 3v_F/4$, where $v_F = \sqrt{2E_F/m_N}$ is the Fermi velocity, with $E_F = 35$ fm and $R = 6$ fm, one gets $\Gamma \simeq 6$ fm. This is the typical energy width a giant dipole resonance state in a heavy nucleus. In the case of neutron-rich light nuclei \bar{v} is not well defined. There are two average velocities: one for the nucleons in the core, \bar{v}_c , and another for the nucleons in the skin, or halo, of the nucleus, \bar{v}_h . One is thus tempted to use a substitution in the form $\bar{v} = \sqrt{\bar{v}_c \bar{v}_h}$. Following ref. [50], the width of

momentum distributions of core fragments in knockout reactions, σ_c , is related to the Fermi velocity of halo nucleons by $v_F = \sqrt{5\sigma_c^2}/m_N$. Using this expression with $\sigma_c \simeq 20$ MeV/c, we get $\Gamma = 5$ MeV (with $R = 3$ fm). This value is much larger than that observed in experiments, as seen in figure 5.

It seems clear that the piston model is not able to describe the width of the response function properly. More microscopic models, e.g. those based on random phase approximation (RPA) calculations [51, 52] are necessary to tackle this problem. The halo nucleons have to be treated in a special way to get the response at the right energy position, and with approximately the right width [49, 52]. The problem remains if the peak in figure 5 is due to a direct transition to the continuum, weighted by the phase space of the fragments, or if it proceeds sequentially via a soft dipole collective state.

B. Limits of the Helm model and alike

The Helm model [53] has become very popular in describing elastic and inelastic electron scattering. This model assumes that the transition density is peaked at the surface. This assumption is justified by the Pauli principle in large, stable, nuclei. In a collective nuclear mode a scattered nucleon attempts to occupy an orbit which is already filled by another nucleon. Thus, low-lying nuclear excitations involve nucleons near the surface where unoccupied orbits are available into which the nucleons may scatter. In the Helm model the transition density is written as

$$\langle f | \rho(\mathbf{r}) | i \rangle = \int \rho_s(\mathbf{r}') \delta\rho_{if}(\mathbf{r} - \mathbf{r}') d^3r, \quad (49)$$

where $\rho_s(\mathbf{r}')$ accounts for the surface layer of the nucleus:

$$\rho_s(\mathbf{r}) = \left(\frac{1}{\pi a^2} \right)^{3/2} \exp \left[-\frac{r^2}{a^2} \right]. \quad (50)$$

The transition density in the Helm model is given by

$$\delta\rho_{if}(\mathbf{r} - \mathbf{r}') = \chi \frac{Ze}{R^2} \delta(r - R) \mathcal{Y}_{J_f M_f}(\mathbf{r}) \mathcal{Y}_{J_i M_i}(\mathbf{r}), \quad (51)$$

where $\mathcal{Y}_{J_i M_i}(\mathbf{r})$ and $\mathcal{Y}_{J_f M_f}(\mathbf{r})$ are spin-angle functions characterizing the initial and final nuclear states. The factor χ was introduced to adjust eq. 51 to the experimentally found

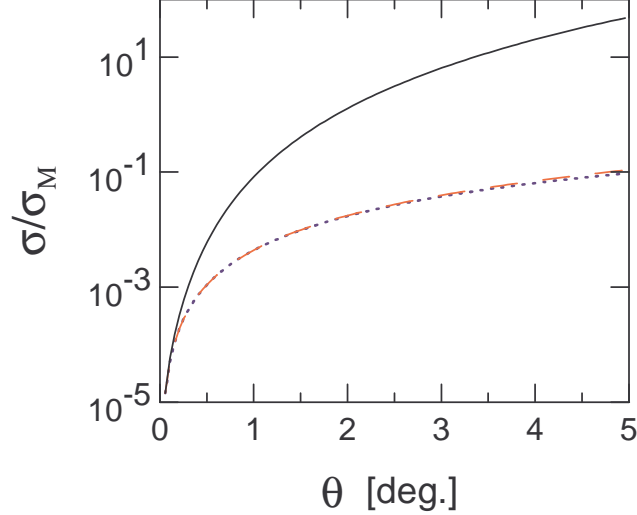


FIG. 9: Angular dependence of the inelastic electron scattering for a state at excitation energy $E_x = 2$ MeV. The continuous curve is obtained with eq. 5. The dashed curve was calculated with the Helm model, eqs. 53 and 54, with $a = 1$ fm and $R = 3$ fm. The cross sections are plotted in terms of their ratio to the Mott cross section, σ_M . The dashed curve is obtained by switching off the second and third terms inside the brackets in eq. 5.

value of the strength function. In this model, the matrix elements for EL transitions in eq. 3 become

$$F_{ij}(q; EL) = \chi Zei^L \langle J_f \parallel Y_L(\hat{\mathbf{r}}) \parallel J_i \rangle j_L(qR) \exp\left[-\frac{q^2 a^2}{4}\right]. \quad (52)$$

Using eq. 19 for a nucleus with $J_i = 0$ and $J_f = L = 1$, one gets for the inelastic electron scattering cross section, neglecting the recoil correction and the terms inside brackets of eq. 5,

$$\left(\frac{d\sigma}{d\Omega}\right)_{inel} = \chi^2 \frac{1}{3} q^2 R^2 \left(\frac{d\sigma}{d\Omega}\right)_{elast}, \quad (53)$$

where

$$\left(\frac{d\sigma}{d\Omega}\right)_{elast} = \frac{27\sigma_M}{q^2 R^2} |j_1(qR)|^2 \exp\left[-\frac{q^2 a^2}{2}\right] \quad (54)$$

is the elastic electron scattering cross section, when the charge of the nucleus is assumed to be homogeneously distributed within a sphere of radius R and a smearing of the surface is accounted for. The factor $\chi^2 q^2 R^2 / 3$ in equation 53 is a rough measure of the fraction of the charge which participates in the inelastic scattering.

If we adapt the Helm model to calculate the response function of eq. 8 then it will also yield a delta-function located at the value of the resonance energy. This is of course not

what is seen in figure 5. But does this matter for electron scattering in electron-ion colliders? To assess this question let us compare the results of eq. 5 with that of eq. 54. We calculate the angular dependence of the inelastic electron scattering for a state at excitation energy $E_x = 2$ MeV. We use eq. 5, and eqs. 6-8. Since in this approach the strength does not depend on the scattering angle, the angular dependence is the same as in eq. 9. In figure 9 we compare this angular dependence with that obtained using the Helm model, eqs. 53 and 54, with $a = 1$ fm and $R = 3$ fm. The cross sections are plotted in terms of their ratio to the Mott cross section, σ_M . Additionally, the recoil term in eq. 5 has been discarded and the strength function has been normalized to the same value in both cases. The solid curve is obtained with eq. 5 while the dashed curve is obtained with the Helm model. One observes that the PWBA result of eq. 5 deviates appreciably from the Helm model as the scattering angle increases. The reason is the presence of the second and third terms inside brackets of eq. 5. If one switches off these terms, instead of the solid curve one gets dotted curve of figure 9. The agreement with the Helm model is then almost perfect. As can be easily verified analytically, in this case the angular dependence of eq. 5 and of eq. 53 become identical (for $\theta \ll 1$). Thus we conclude that the angular dependence of the inelastic cross section in the Helm model is of limited value for $\theta \ll 1$.

The Helm model is not appropriate to describe the excitation energy dependence in inelastic scattering cross section off halo nuclei. The reason is that, as clearly seen in figure 8, the transition densities in such nuclei are not so strongly peaked at the surface that a delta-function approximation is justifiable. The smearing factor $\exp(-q^2 a^2/2)$ introduced in the Helm model does not really have anything to do with the transition density and can be used at most as a fitting procedure. Other models, e.g. the Tassie and the Bohr-Mottelson models [13], also suffer from the same problems. They are based on derivatives of the nuclear ground state densities. Despite the fact that they yield good results for large stable nuclei, they fail to describe the transition densities in light, unstable nuclei, due to their extended matter distribution and cluster aspects.

V. SUMMARY AND CONCLUSIONS

We have studied the feasibility to determine the low energy excitation properties of light, exotic, nuclei from experimental data on inelastic electron scattering in an electron-ion col-

lider mode. It was shown that for the conditions involved in the collider mode, the electron scattering cross sections are directly proportional to the same electromagnetic matrix elements involved in photonuclear processes with real photons. This proportionality is lost when larger scattering angles, and a larger ratio of the excitation energy to the electron energy, E_γ/E , are involved.

Proper equations for electron scattering cross sections have been developed. The differential cross section for the emission of fragments at a given angle with respect to the incident beam has been also studied. In this case, the longitudinal and transverse components of the electromagnetic field of the electron appear mixed. The proportionality between electron scattering and scattering by real photons is only recovered after the integration over the emitted angle of the particle is performed and for $E_\gamma/E \ll 1$.

One of the important issues to be studied in future electron-ion colliders is the nuclear response at low energies. This response can be explained in two ways: by a (a) direct breakup and by a (a) collective excitation. We have shown that in the case of direct breakup the response function will depend quite strongly on the final state interaction. This may become a very useful technique to obtain phase-shifts, or effective-range expansion parameters, of fragments far from the stability line. In the case of collective excitations, a variant of the Goldhaber-Teller and Steinwedel-Jensen model was used to obtain the transition densities in halo nuclei. The transition density obtained in this model is similar to what is obtained in few-body models. However, the model predicts a well defined resonance energy. An attempt to describe the width of the response function in the hydrodynamical model is shown to be unreliable.

The limits of application of the Helm model were also studied. It has been shown that the model cannot be directly applied to the description of excitation of soft dipole modes in light, neutron-rich nuclei. But the model works quite well to describe the angular dependence of energy integrated differential cross sections, as long as modifications in the elastic scattering cross sections are introduced.

The pygmy resonance lies above the neutron emission threshold, effectively precluding its observation in (γ, γ') experiments on very neutron-rich nuclei. Nonetheless, electron scattering experiments will probe the response function under several conditions, including different bombarding energies, different scattering angles, etc. The study of pygmy resonances and of final state interactions will certainly be an important line of investigation in these facilities.

Acknowledgments

The author is grateful to Haik Simon for useful discussions. This work was supported by the U.S. Department of Energy under grant No. DE-FG02-04ER41338.

- [1] C.A. Bertulani, M.S. Hussein, and G. Münzenberg, *Physics of Radioactive Beams* (Nova Science Publishers, Hauppauge, NY, 2002).
- [2] I. Tanihata et al., Phys. Rev. Lett. **55** (1985) 2676.
- [3] G.Baur, C.A.Bertulani and H.Rebel, Nucl. Phys. **A458** (1986) 188.
- [4] C.A.Bertulani and G.Baur, Phys. Reports **163** (1988) 299.
- [5] N. Takigawa and H. Sagawa, Phys. Lett. **B 265** (1991) 23.
- [6] M. S. Hussein et al., Phys. Rev. **C 46** (1992) 377.
- [7] J. Hardy, in *Physics of Unstable Nuclear Beams*, Edited by C.A.Bertulani et al., World Scientific, Singapore, 1997.
- [8] P. Danielewicz, R. Lacey and W. G. Lynch, Science **298**, 1592 (2002).
- [9] Haik Simon, *Technical Proposal for the Design, Construction, Commissioning, and Operation of the ELISe setup*, GSI Internal Report, Dec. 2005.
- [10] T. Suda, K. Maruayama, *Proposal for the RIKEN beam factory*, RIKEN, 2001; M. Wakasugia, T. Suda, Y. Yano, Nucl. Inst. Meth. Phys. **A 532**, 216 (2004).
- [11] A.N. Antonov et al., Phys. Rev. **C72**, 044307 (2005).
- [12] C.A. Bertulani, Los Alamos archive, nucl-th/0604044.
- [13] C.A. Bertulani, L.F. Canto and M.S. Hussein, Phys. Reports **226**(1993) 281.
- [14] A. Leistenschneider et al., Phys. Rev. Lett. **86**, 5442 (2001).
- [15] C.A.Bertulani, Phys. Rev. Lett. **94**, 072701 (2005).
- [16] K. Ieki et al., Phys. Rev. Lett. **70**, 730 (1993).
- [17] D. Sackett et al., Phys. Rev. **C 48**, 118 (1993).
- [18] H. Sagawa et al., Z. Phys. **A 351**, 385 (1995).
- [19] M.S. Hussein, C.Y Lin and A.F.R. de Toledo Piza, Z. Phys. **A 355** (1966) 165.
- [20] S. Goriely, Phys. Lett. **B 436** (1998) 10.
- [21] W.C. Barber, Ann. Rev. Nucl. Sci. **12**, 1 (1962).

[22] J.M. Eisenberg and W. Greiner, “Excitation Mechanisms of the Nucleus”, (North-Holland, Amsterdam, 1988).

[23] A.J.F. Siegert, Phys. Rev. **52**, 787 (1937).

[24] R.G. Sachs and N. Austern, Phys. Rev. **81**, 705 (1951).

[25] L.I. Schiff, Phys. Rev. **96**, 765 (1954).

[26] B. Bosco and S. Fubini, Nuovo Cimento **9** (1964) 527.

[27] J.M. Eisenberg, Phys. Rev. **132**, 2243 (1963).

[28] C.A. Bertulani and G. Baur, Nucl. Phys. **A480**, 615 (1988).

[29] C.A. Bertulani and A. Sustich, Phys. Rev. **C 46**, 2340 (1992).

[30] T. Otsuka et al., Phys. Rev. **C 49**, R2289 (1994).

[31] A. Mengoni, T. Otsuka and M. Ishihara, Phys. Rev. C **52**, R2334 (1995).

[32] D.M. Kalassa and G. Baur, J. Phys. **G 22**, 115 (1996).

[33] S. Typel and G. Baur, Phys. Rev. Lett. **93**, 142502 (2004).

[34] C.A. Bertulani and P. Danielewicz, *Introduction to Nuclear Reactions* (IOP Publishing, Bristol, UK, 2004).

[35] R.A. Arndt, D.L. Long, L.D. Roper, Nucl. Phys. **A209** (1973) 429.

[36] M. V. Zhukov, B.V. Danilin, D.V. Fedorov, J.M. Bang, I.J. Thompson and J.S. Vaagen, Phys. Rep. **231**, 151 (1993).

[37] S.P. Merkuriev, Sov. J. Nucl. Phys. **19** (1974) 222.

[38] A Pushkin, B Jonson and M V Zhukov, J. Phys. **G 22** (1996) L95.

[39] L.V. Chulkov, B. Jonson and M.V. Zhukov, J. Phys. **G 22** (1996) 95.

[40] C. Forssen, V.D. Efros and M.V. Zhukov, Nucl. Phys. **A 697** (2002) 639.

[41] C. Forssen, V.D. Efros and M.V. Zhukov, Nucl. Phys. **A 706** (2002) 48.

[42] C. A. Bertulani, G. Baur and M. S. Hussein, Nucl. Phys. **A 526** (1991) 751.

[43] M. Thoennessen et al., Phys. Rev. **C 59**, 111 (1999).

[44] S. Shimoura et al., Phys. Lett. **B 348** (1995) 29.

[45] Y. Suzuki, K. Ikeda, and H. Sato, Prog. Theor. Phys. **83**, 180 (1990).

[46] M. Goldhaber and E. Teller, Phys. Rev. **74**, 1046 (1948).

[47] H. Steinwedel and H. Jensen, Z. Naturforschung **5A**, 413 (1950).

[48] W.D. Myers, W.G. Swiatecki, T. Kodama, L.J. El-Jaick and E.R. Hilf, Phys. Rev. **C 15**, 2032 (1977).

- [49] H. Sagawa and C.A. Bertulani, *Prog. Theo. Phys. Suppl.* **124**, 143 (1996).
- [50] C.A. Bertulani and K.W. McVoy, *Phys. Rev. C* **48** (1993) 2534.
- [51] G.F. Bertsch and J. Foxwell, *Phys. Rev. C* **41** (1990) 1300.
- [52] N. Teruya, C.A. Bertulani, S. Krewald, H. Dias, and M.S. Hussein, *Phys. Rev. C* **43** (1991) R2049.
- [53] R.H. Helm, *Phys. Rev.* **104**, 1466 (1956).